VALIDATION OF BALLISTIC SHOCK PREDICTION MODELS AND TECHNIQUES FOR USE IN THE CRUSADER COMBAT VEHICLE PROGRAM (U)

Brent Loper
Military Technologies, Inc.
6767 Old Madison Pike, Bldg. 2, Suite 200
Huntsville, AL 35806
(256) 971-1970

Abraham Frydman, Morris Berman, and Dean Li
Army Research Laboratory
Adelphi, MD

ABSTRACT (U)

(U) For the past ten to fifteen years, the combat vehicle community has recognized the necessity of considering ballistic shock effects into new vehicle designs. This necessity arose from concern for sensitive electronic components in modern vehicles, and new classes of vehicles utilizing lightweight composite structures. Also, live-fire and other ground tests conducted with modern instrumentation have proven the damage potential of ballistic shock. Despite the recognized need for ballistic shock design as cited, analysis to support these designs with shock predictions has been slow in becoming standard throughout the industry. This slow trend is due mostly to the unwieldy nature of common transient response tools, such as finite element methods, for such complex structures and frequency ranges involved. The Army Research Laboratory (ARL), in conjunction with Military Technology, Inc., has been investigating the use of more tractable numerical methods and disciplined system engineering approaches to support ballistic shock design. As a prelude to the characterization of ballistic shock effects on a full-scale vehicle, the Crusader Program has sponsored a ballistic test of a surrogate structure representing a vehicle front section, with a simulated component and mounting structure. The aim of the test is to evaluate the effectiveness of the method by directly comparing analysis results with measured response values, and finite element predictions. This paper will outline the analysis procedure and display the model and test result comparisons.

(U) INTRODUCTION

(U) The U.S Army is investigating the use of aluminum and composites to reduce weight in future generations of lightweight armored vehicles. To design survivable components for this new vehicle class, it is necessary to understand the transmission of ballistic shock, and to have the ability to predict shock levels in these complex structures. Because of the high frequency range of ballistic shock, conventional analysis methods such as finite element analysis (FEA) can become intractable, especially for large structures. Because of this limitation, the Army Research Laboratory, with Military Technology, Inc. as the principal support contractor, have been investigating an analysis method using statistical energy analysis (SEA) for the prediction of ballistic shock in combat vehicles [1,2,3]. When compared to conventional analysis methods, this method results in faster model construction, smaller model sizes, faster run times, and a reduced set of input parameters. This reduced set of parameters enables models to be easily tuned from measured parameters, a valuable property due to the difficulty of directly modeling the shock transmission through exotic materials and joining concepts [3,4].

(U) The shock prediction method uses an algorithm called virtual mode synthesis and simulation (VMSS). VMSS is used to develop dynamic response equations by curve-fitting coupled modal frequency response

functions (FRF) to an FRF magnitude that originates from energy balance models (e.g., statistical energy analysis) or non-destructive tests. The curve fitting process results in a set of mathematical coefficients that are referred to as the virtual modes of the system. The transient response is then predicted by modal summation using numerical integration with an estimate of the ballistic contact load history. The technique is shown graphically in Figure 1.

(U) This paper will describe an implementation of this method on a structure representing a section of the Crusader combat vehicle. The analysis reported here simulates a series of ballistic impact tests conducted using this structure. The contact load was predicted using the CTH impact physics code, damping was calculated using a small finite element model, and the shock response predicted using the methods described above. The paper contains a brief description of the SEA and VMSS methods, with complete descriptions of the methods given in [5,6]. Comparisons of the predicted shock results to measured test data are also included, as well as comparisons to results obtained using a finite element model.

(U) TEST ARTICLE DESCRIPTION

(U) A series of ballistic tests conducted by the Impact Physics Branch of ARL were designed to simulate a fragment impacting the front corner section of the Crusader vehicle. The purpose of these tests was to measure ballistic shock response at an internal component, and compare these measurements to analysis predictions. The test article (Figure 2), called the Combat Ground Vehicle-Front End Surrogate Subsection (CGV-FESS), was constructed entirely of aluminum except for Kevlar spall liners and a steel plate to simulate top attack armor. The aluminum plates comprising the sides and front of the structure were 1.5" thick, and the top was 1" thick. The bottom surface was 0.6" and 1.0" thick. The structure was welded at all joints. The spall liners were attached to the top and side plates with flexible adhesive and bolts. The test article was bolted to a steel test fixture along the inboard edge through large angle iron beams. The angle iron was attached to a vertical steel plate, which was in turn attached to a thick steel base. The vertical plate was reinforced with large angle iron beams. Response measurements were taken at gages on the side, front plate, and sponson bottom. Shock response predictions were made at the front plate and sponson locations.

Figure 2 (U) CGV-FESS Test Article; View From Front Outboard.

(U) A simulated electro-mechanical component was mounted to the front floor of the test article (Figure 3). The box-like enclosure for the component was constructed from 0.25" and 0.375" aluminum plates. The box was welded on four sides, with the inboard and outboard sides bolted at four locations. Five mass simulators were mounted to the bottom of the box as shown in the schematic in Figure 4. Three sets of response gages were located inside the box, two on the base of the box and one on the top of the center mass. Shock response predictions were

made at the inboard base gage location. The component was attached to an aluminum tray structure through two bolts and two shear pins. This tray was in turn bolted to the floor through four stand-offs.

Figure 3 (U) CGV-FESS Test Article; Interior View.

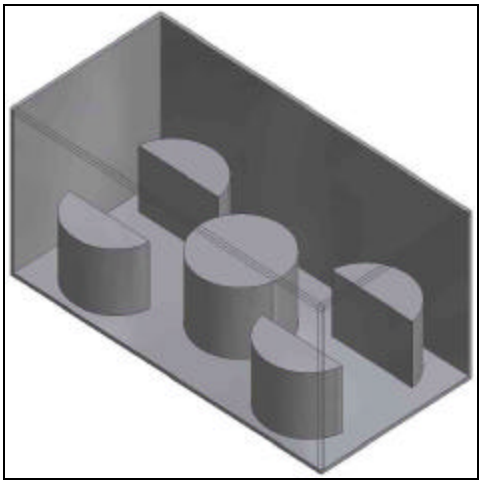

Figure 4 (U) Schematic of CGV-FESS Simulated Component Showing Location of Mass Simulators and Response Gages.

(U) VMSS ALGORITHM DESCRIPTION

(U) The transient dynamic response described in this paper is based on the method of modal superposition and numerical integration. Damping, mode density, and frequency response function magnitude can be estimated or measured in various ways, but the mode shapes are usually unknown. For the method described here, this vital piece of information is estimated using the Virtual Mode Synthesis approach, which is implemented using the PowerSurge software developed by Military Technology, Inc.

(U) In general, the mode synthesis process can be used to estimate the virtual mode coefficients for either an envelope or frequency band averaged FRF magnitude. The FRF estimate can be either measured or predicted with some analytical tool. In the context of this paper, the FRF and other data is provided directly from an SEA model, therefore, the input FRF is in a frequency band averaged form.

(U) Virtual modes can be roughly defined as approximations of the actual physical modes under the key assumption of full-diagonal decoupling. The result of the mode synthesis process is a vector containing approximations to the mode shape coefficient products for the i^{th} response and j^{th} force at each virtual mode frequency. This vector is written as

$$\{\Phi\}_{ij} = \begin{Bmatrix} f_{i1} f_{j1} \\ f_{i2} f_{j2} \\ \vdots \\ f_{in_m} f_{jn_m} \end{Bmatrix} \tag{1}$$

(U) The main property of the synthesized dynamical system sought is that the FRF magnitude approximates the measured or predicted FRF envelope or band average. In other words, the virtual modes are not pure physical entities, but rather mathematical coefficients of the same form that produce an FRF mapping to the desired (measured or predicted) FRF. Whether the envelope or band average is approximated depends on the method of mode synthesis selected.. Although the band average method is used in this analysis, both methods will be discussed here.

(U) FRF Envelope Approximation

(U) The magnitude of the frequency response is found by taking the square root of the sum of the squares of the real and imaginary parts of the modal response (in frequency domain). The FRF magnitude is written as

$$\begin{aligned} \left|H_{ij}(\Omega)\right| &= \left| \sum_{m=1}^{n_m} f_{im} f_{jm} \frac{\left(w_m^2 - \Omega^2 - 2z_m w_m \Omega i\right)}{\left(w_m^2 - \Omega^2\right)^2 + \left(2z_m w_m \Omega\right)^2} \right| \\ &= \left[\left(\sum_{m=1}^{n_m} \frac{f_{im} f_{jm} \left(w_m^2 - \Omega^2\right)}{\left(w_m^2 - \Omega^2\right)^2 + \left(2z_m w_m \Omega\right)^2} \right)^2 + \left(\sum_{m=1}^{n_m} \frac{f_{im} f_{jm} 2z_m w_m \Omega}{\left(w_m^2 - \Omega^2\right)^2 + \left(2z_m w_m \Omega\right)^2} \right)^2 \right]^{1/2} \end{aligned} \tag{2}$$

where ζ is the modal damping, Ω is the driving force frequency, ω_m is the modal frequency, m is the mode index, and n_m is the number of virtual modes (derived from the mode density). This system is non-linear with respect to the virtual modes, and cannot be solved with a simple matrix inverse. As an alternative, the modal frequency response can also be written in time domain as the sinusoidal response of a multi-modal system to a sinusoidal input of frequency Ω. The general form of the velocity time response is written as

$$\begin{aligned} v_{ij}(\Omega, t) &= \sum_{m=1}^{n_m} f_{im} f_{jm} R_m(\Omega, t) \\ &= \sum_{m=1}^{n_m} f_{im} f_{jm} \Omega \left\{ \frac{1}{\sqrt{c}} \sin\left(\Omega t + j\right) + \frac{1}{b} \left(\frac{a^2 + b^2}{c} \right)^{1/2} e^{-at} \sin\left(bt + g\right) \right\}_m \end{aligned} \tag{3}$$

where

$$\begin{aligned} a &= z_m w_m, & j &= \frac{p}{2} - \tan^{-1} \frac{2a\Omega}{a^2 + b^2 + \Omega^2}, \\ b^2 &= w_m^2 \left(1 - z_m^2\right), & g &= \tan^{-1} \frac{b}{-a} + \tan^{-1} \frac{2ab}{a^2 - b^2 + \Omega^2} \\ c &= \left(2a\Omega\right)^2 + \left(a^2 + b^2 - \Omega^2\right)^2 \end{aligned} \tag{4}$$

(U) The time domain response shown in Eq. (3) is equivalent to the FRF magnitude when evaluated at some time t_{max} such that a peak response is produced (Figure 5). The transient portion of the response can be ignored for the current discussion.

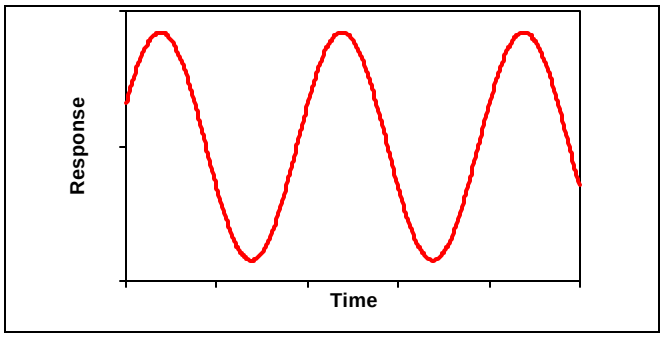

Figure 5 (U) Evaluation Time for Maximum Steady-State Response of Multi-Modal System

(U) Eq. (3) can be evaluated at t_{max} and written as the product of two vectors, which yields

$$v_{ij}(\Omega, t_{\max}) = \left\lfloor R(\Omega, t_{\max}) \right\rfloor \left\{\Phi\right\}_{ij} \tag{5}$$

where R is written as

$$\left\lfloor R(\Omega, t_{\max}) \right\rfloor = \left[\frac{\Omega}{\sqrt{c_1}} \sin\left(\Omega t_{\max} + j_1\right) \quad \frac{\Omega}{\sqrt{c_2}} \sin\left(\Omega t_{\max} + j_2\right) \quad \cdots \quad \frac{\Omega}{\sqrt{c_{n_m}}} \sin\left(\Omega t_{\max} + j_{n_m}\right) \right] \tag{6}$$

Evaluating the frequency response at the virtual mode frequencies results in a matrix expression relating the FRF magnitude to the virtual modes. Assuming the value of t_{max} corresponds to the peak response, the velocity response is replaced with the input FRF magnitude and written as

$$\left\{\left|H(\Omega)\right|\right\}_{ij} = \mathbf{R}\left\{\Phi\right\}_{ij} \tag{7}$$

where

$$\left\{\left|H(\Omega)\right|\right\}_{ij} = \begin{Bmatrix} \left|H(\Omega_1 = \omega_1)\right| \\ \left|H(\Omega_2 = \omega_2)\right| \\ \vdots \\ \left|H(\Omega_{n_m} = \omega_{n_m})\right| \end{Bmatrix}_{ij} \quad \text{and} \quad \mathbf{R} = \begin{Bmatrix} \lfloor R(\Omega_1, t_{\max 1})\rfloor \\ \lfloor R(\Omega_2, t_{\max 2})\rfloor \\ \vdots \\ \lfloor R(\Omega_{n_m}, t_{\max n_m})\rfloor \end{Bmatrix}_{ij} \tag{8}$$

(U) The difficulty in finding a solution for the virtual mode coefficients is due to $2n_m$ unknowns and n_m equations, with the solution for t_{max} being non-linear. The approach for a solution is to assume values for the virtual mode coefficients, solve for a vector of times (one value of t_{max} for each forcing frequency Ω), and use these times to solve for a new set of virtual mode coefficients. The expression for t_{max} is found by first rewriting Eq. (3) as

$$v_{ij}(\Omega_k, t_{\max}) = \sum_{m=1}^{n_m} \phi_{im}\phi_{jm}\frac{\Omega_k}{\sqrt{c_m}}\left\{\cos\psi_m \sin(\Omega_k t_{\max}) + \sin\psi_m \cos(\Omega_k t_{\max})\right\}. \tag{9}$$

At a peak in the sinusoidal response, the time derivative of the velocity response is zero. Taking the derivative of Eq. (9), setting to zero, and solving for t_{max} results in

$$t_{\max}(\Omega_k) = \tan^{-1}\left(\frac{\sum_{m=1}^{n_m}\phi_{im}\phi_{jm}\frac{\cos\psi_m}{\sqrt{c_m}}}{\sum_{m=1}^{n_m}\phi_{im}\phi_{jm}\frac{\sin\psi_m}{\sqrt{c_m}}}\right)_k \tag{10}$$

The **R** matrix of Eq. (7) is evaluated using the times from Eq. (10), and the virtual mode coefficients found by matrix inversion, written as

$$\left\{\Phi\right\}_{ij} = \mathbf{R}^{-1}\left\{\left|H(\Omega)\right|\right\}_{ij} \tag{11}$$

(U) The FRF produced using the virtual mode coefficients is then compared to the input FRF using a convergence criteria of % difference. If convergence is not reached, the process is repeated, starting with calculating the times of maximum response with the virtual mode coefficients found in the previous step. The smaller the convergence criteria, the more closely the solutions will eventually match, although this may result in many iterations. This iterative scheme is shown graphically in Figure 6.

(U) FRF Band Average Approximation

(U) For the case of a band average input FRF, the frequency response is evaluated at sufficient frequencies Ω_k to "map" the peaks and valleys of the synthesized FRF. The rows of the **R** matrix of Eq. (6) now correspond to these mapping frequency increments, and must be evaluated at separate values of t_{max}. The system of equations for this method are written as

$$\hat{\mathbf{a}}\,\mathbf{S}\,\mathbf{R}^T\left\{\Phi\right\}_{ij} = \mathbf{B}\left\{\Phi\right\}_{ij} = \left\{\mathrm{H}(\Delta\omega)\right\} \tag{12}$$

with one element of **R** corresponding to a mapping frequency increment (row) k and virtual mode frequency (column) m written as

$$R_{k,m} = \frac{1}{2}\left[\frac{\Omega_k}{\sqrt{c_{k,m}}}\sin(\Omega_k t_{\max} + \psi_{j,m}) + \frac{\Omega_{k+1}}{\sqrt{c_{k+1,m}}}\sin(\Omega_{k+1} t_{\max} + \psi_{k+1,m})\right] \tag{13}$$

The $\hat{\mathbf{a}}$ and **S** matrices are used to implement the averaging process, and are written as

$$\hat{\mathbf{a}} = \begin{bmatrix} 1/\Delta w_1 & & & & \\ & 1/\Delta w_2 & & \mathbf{0} & \\ & & 1/\Delta w_3 & & \\ & \mathbf{0} & & \ddots & \\ & & & & 1/\Delta w_N \end{bmatrix}, \tag{14}$$

$$\mathbf{S} = \begin{bmatrix} (\Delta\Omega_1)_1 \;\; (\Delta\Omega_2)_1 \;\cdots\; (\Delta\Omega_{n_1-1})_1 & & & \\ & (\Delta\Omega_1)_2 \;\; (\Delta\Omega_2)_2 \;\cdots\; (\Delta\Omega_{n_2-1})_2 & & \mathbf{0} \\ \mathbf{0} & & \ddots & \\ & & & (\Delta\Omega_1)_N \;\; (\Delta\Omega_2)_N \;\cdots\; (\Delta\Omega_{n_N-1})_N \end{bmatrix} \tag{15}$$

where n_n is the number of mapping frequencies in frequency band n, and

$$\Delta\Omega_k = (\Omega_{k+1} - \Omega_k). \tag{16}$$

Using Eq. (12) results in trapezoidal rule integration across the frequency band with n_n discrete points. In general, the number of frequency bands will be much less than the number of virtual modes, resulting in a system of fewer equations than unknowns. This system can be solved using a pseudo-inverse by the minimum norm method, which yields

$$\{\Phi\}_{ij} = \mathbf{B}^* \{|H|\}_{ij} \tag{17}$$

where

$$\mathbf{B}^* = \mathbf{B}\left(\mathbf{B}^T\mathbf{B}\right)^{-1} \tag{18}$$

The resulting Φ vector elements are synthesized, virtual mode coefficients (modal gain), i.e., the $f_{im} f_{jm}$. Note that this solution vector is not unique, but yields the same band average as the input FRF.

(U) SEA MODEL DESCRIPTION

(U) The elements of a SEA model are subsystem components such as walls, bulkheads, floors, etc., that are interconnected by structural discontinuities (joints). SEA models the flow of vibrational power among the elements by a thermodynamic analogy that distributes an average amount of power from individual vibration modes of the elements to the modes of the connected elements.

(U) The vibrational power balance provided by SEA for a bandwidth Δw may be written,

$$\{p(w)\} = w\mathbf{C}(w)\{E(w)\} \tag{19}$$

where $p_i(w)$ is the input power to the i^{th} element, w is the center band frequency, and $E_i(w)$ is the energy of the i^{th} element ($\{p\}$ and $\{E\}$ are column vectors.) The matrix $\mathbf{C}(w)$ has the form

$$\mathbf{C}(w) = \begin{bmatrix} \eta_{1,TOT} & -\eta_{2,1} & -\eta_{3,1} & \cdots & -\eta_{J,1} \\ -\eta_{1,2} & \eta_{2,TOT} & -\eta_{3,2} & \cdots & -\eta_{J,2} \\ -\eta_{1,3} & -\eta_{2,3} & \eta_{3,TOT} & \cdots & -\eta_{J,3} \\ \vdots & \vdots & \vdots & \ddots & \vdots \\ -\eta_{1,J} & -\eta_{2,J} & -\eta_{3,J} & \cdots & \eta_{J,TOT} \end{bmatrix} \tag{20}$$

where the off-diagonal terms are so-called coupling loss factors $\eta_{i,j}(w)$ which describe the flow of energy among elements. The diagonal terms are composed of the sum of the same column (but with positive signs) and the so-

called element loss factor η_i which describes the energy loss of an element due to damping (η = two times the percent critical damping).

(U) To extract the FRF, the energy variables of the power balance must first be re-expressed in terms of the physical parameters of force and response. The energy of a randomly vibrating plate may be expressed in terms of the time and spatially averaged velocity squared $\langle \bar{v}_i^2 \rangle$ times the element mass M_i,

$$E_i = \langle \bar{v}_i^2 \rangle M_i \tag{21}$$

The input power to an element may be expressed as the mean-squared force times the real part of the load admittance function (LAF) $Y(\omega)$ (the driving point FRF),

$$\pi_i(\omega) = \langle F_i^2 \rangle Y_i(\omega) \tag{22}$$

Substituting Eq.s (21) and (22) into (19), and rearranging,

$$\{\langle \bar{v}^2 \rangle\} = \frac{1}{\omega} \mathbf{M}^{-1}\mathbf{C}^{-1}\mathbf{Y}\{\langle F^2 \rangle\} \tag{23}$$

where **M** and **Y** are diagonal matrices.

By dividing both sides of Eq. (23) by the bandwidth we obtain, approximately,

$$\{P_v\} = \mathbf{T}\{P_F\} \tag{24}$$

where $\{P_v\}$ is the power spectral density (PSD) of the response velocity, and $\{P_F\}$ is the PSD of the input loading function and

$$\mathbf{T} = \frac{1}{\omega} \mathbf{M}^{-1}\mathbf{C}^{-1}\mathbf{Y} \tag{25}$$

We compare Eq. (24) to the theorem in random vibration theory for uncorrelated input signals,

$$\{P_{out}\} = [|H(\omega)|^2]\{P_{in}\} \tag{26}$$

where $[|H(\omega)|^2]$ is a matrix of the FRF magnitudes squared. The FRF estimates are then approximately the matrix elements given by

$$|\bar{H}(\omega)| = \mathbf{T}^{1/2} \tag{27}$$

(U) It is important to note that the response variable in Eq. (27) is the spatially averaged response velocity (hence the bar notation). The FRF magnitude for a discrete location is provided by operating on the spatially averaged FRF with a response concentration function (RCF), expressed by (on the i^{th} element and j^{th} loaded element)

$$H_{ij}(\omega)_{x,y} = R_{ij}(\omega)\bar{H}_{ij}(\omega) \tag{28}$$

where $R_{ij}(\omega)$ is the RCF and x,y are local plate coordinates of the discrete location. Also, the load admittance variable in Eq. (22) is a space-averaged variable that can be discretized in a manner similar to Eq. (28).

(U) SEA MODEL

(U) The SEA model of the CGV-FESS structure was constructed using the AutoSEA2 software package, which allows the user to graphically represent the model as a three-dimensional image. Construction of the AutoSEA2 model took approximately 2 days, with an additional 2 days for refinement. The model consists of 25 subsystems and FRFs were calculated in under 1minute. The model is shown in Figure 7.

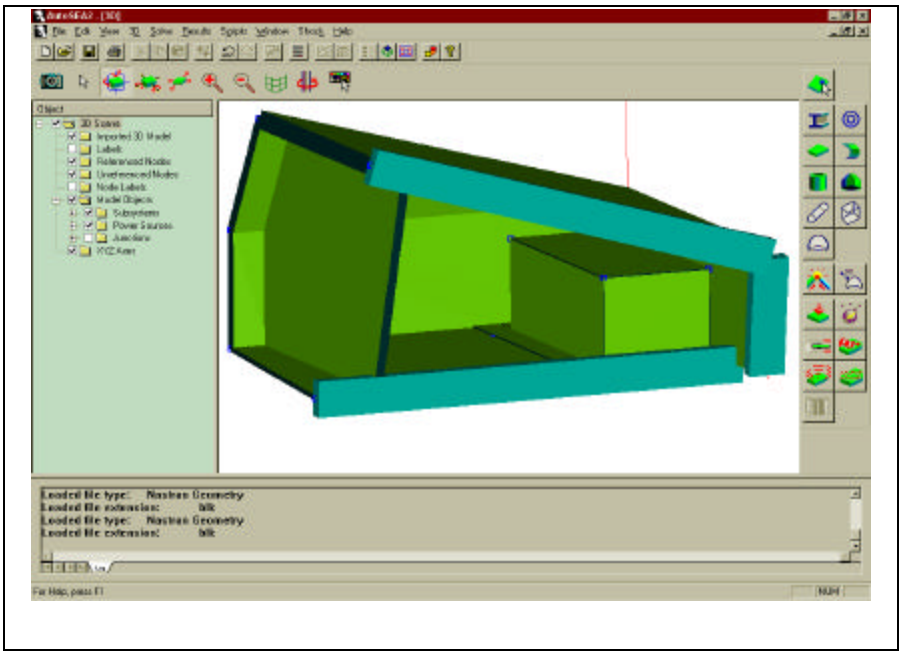

Figure 7 (U) AutoSEA2 Model of CGV-FESS Test Article.

(U) FINITE ELEMENT MODEL

(U) A finite element model of the CGV-FESS structure was constructed using the ANSYS software package. The model consists of approximately 50000 degrees of freedom (DOF), and took approximately 1 month to construct, with additional days for refinement. The transient response calculations to 10000Hz took approximately 24 hrs on a 500MHz Pentium PC. The model is shown in Figure 8.

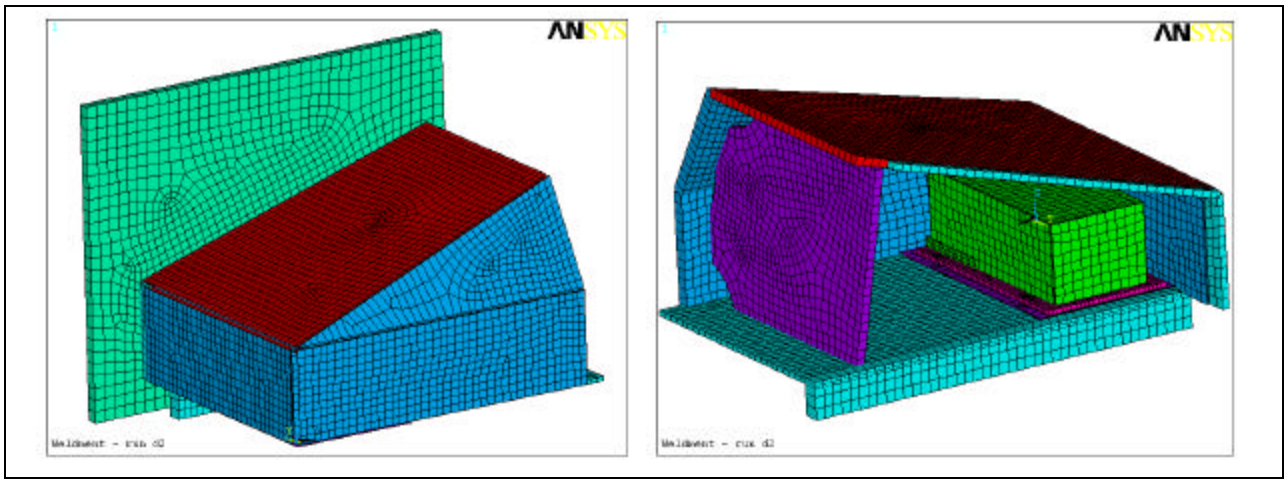

Figure 8 (U) ANSYS Finite Element Model of CGV-FESS Test Article.

(U) CONTACT FORCE ESTIMATION

(U) In order to predict ballistic shock, an estimate of the impact load must be obtained, either from test or analysis. In these tests, the 1.5" aluminum front and side plates were hit with a fragment simulating projectile. Due to the severity of the impact, direct measurements of the force were not possible. As an alternative, the CTH hydrocode was used to simulate the impact event and to predict the momentum time history of the projectile. The momentum was then differentiated with respect to time to yield a force time history. Figure 9 shows a notional hydrocode simulation, and Figure 10 shows the resulting force for the given test conditions.

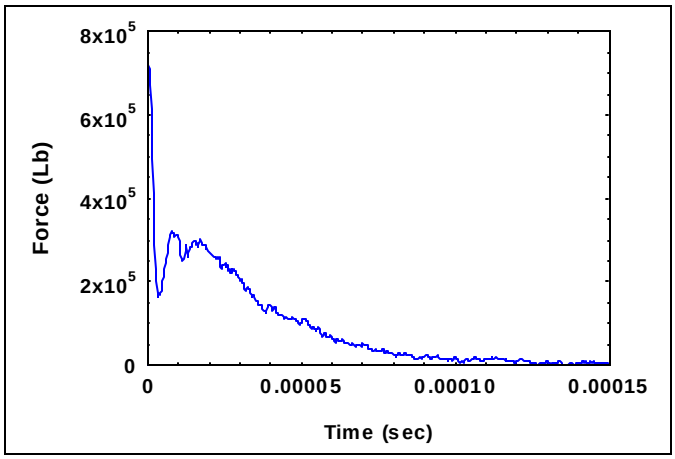

Figure 9 (U) Notional CTH Hydrocode Simulation of Fragment Impact.

Figure 10 (U) Predicted Impact Force for CGV-FESS Ballistic Test Conditions.

(U) SUBSYSTEM DAMPING ESTIMATION

(U) As shown in [4], damping is perhaps the most important property necessary to accurately model a structure with SEA. Unfortunately, measuring damping at high frequency is not a simple matter, and in the case of the CGV-FESS structure, no subsystem damping measurements were attempted. For the bare plates (no spall liner), a damping ratio of 0.1% was assumed for all frequencies. Light damping is a characteristic of orthotropic metallic plates with no wires, components or damping treatments. The damping for the plates with spall liner was estimated using the modal strain energy method [7]. The Kevlar spall liners are attached to the plates with a flexible, visco-elastic adhesive, thus producing a constrained layer damping effect. As the plate bends under flexure, the shear strain in the visco-elastomer results in an energy loss proportional to the material loss factor. The modal strain energy method assumes that the damping loss factor for a given mode is directly proportional to the ratio of modal strain energy in the visco-elastomer and in the entire structure. This method is readily implemented with a finite element model where the modal loss factor is defined as

where: i = mode index $\quad j$ = element index
η_j = element loss factor $\quad \eta_i$ = modal loss factor (29)
ESE = element strain energy

A finite element model (FEM) of a plate with characteristic dimensions for the CGV-FESS was constructed for both the 1.0" and 1.5" thickness. The FEMs included solid elements representing the adhesive layer, and plates representing the Kevlar constraining layer and the aluminum plate. The FEM is shown in Figure 11, and the resulting damping curves in Figure 12.

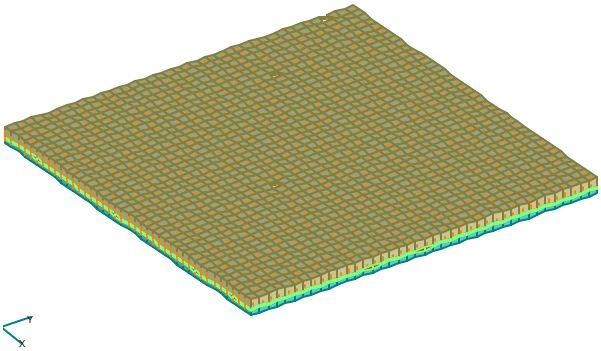

Figure 11 (U) Finite Element Model of Representative CGV-FESS Aluminum Plate with Spall Liner.

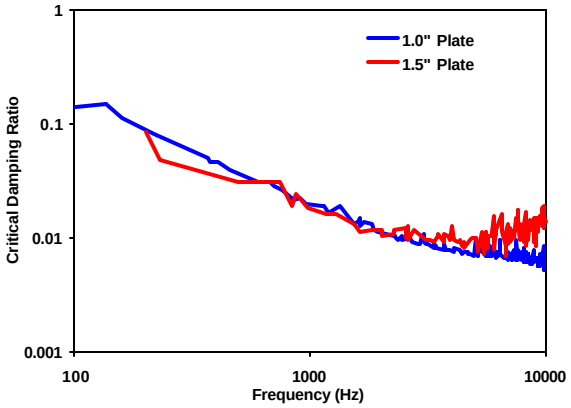

Figure 12 (U) Predicted Damping Spectra for Plates with Spall Liner

(U) SHOCK RESPONSE PREDICTIONS

(U) Using the methods described above, response predictions were made at the inboard measurement location inside the component box, on the inside of the front plate, and on bottom of the sponson front plate. FEA results were not available for the component base location. The FRF magnitude was supplied from the AutoSEA2 model, subsystem damping from the FEM using the modal strain energy method, and the synthesized modes and transient response from PowerSurge. Responses predictions normal to the component base were made for both a side and front impact case using the loading function produced from the hydrocode. The predicted responses are shown in Figures 13 through 18.

(U) The FEA and PowerSurge predicted responses at the front plate and sponson bottom are similar in shape and magnitude to the measurements. In general, the predictions are higher in magnitude, probably as a result of incorrect damping values, and non-linearity in the structure. The predictions at the component base disagreed significantly from the measurements. The differences are most likely attributed to non-linear structural attachments between the component and the tray. The box base actually rests atop the support tray, but is attached only at four point locations. The linear modeling practices described in this paper cannot simulate this partial contact behavior. Note also that the predictions shown here are the result of models that have not been modified to improve the comparison.

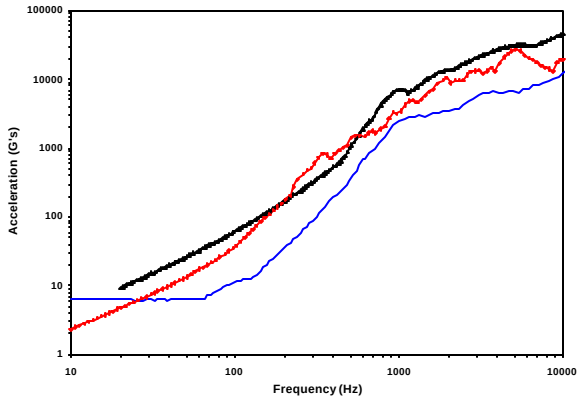

Figure 13 (U) Predicted vs Measured SRS at Front Plate for Front Impact on CGV-FESS.

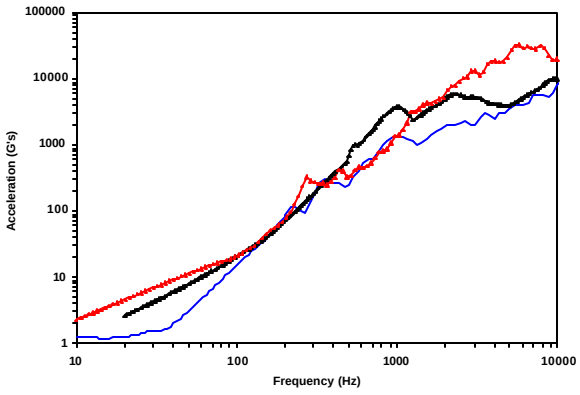

Figure 14 (U) Predicted vs Measured SRS at Sponson Front for Front Impact on CGV-FESS.

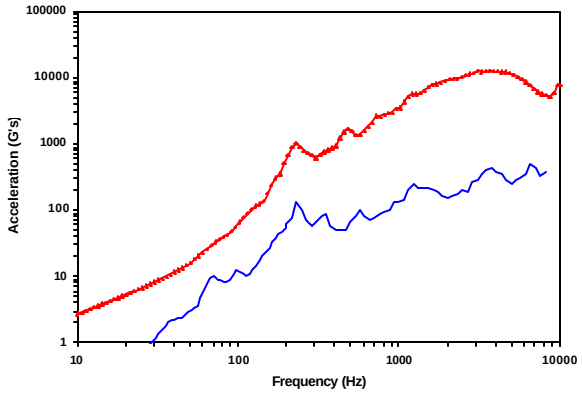

Figure 15 (U) Predicted vs Measured SRS at Inbd. Component Base for Front Impact on CGV-FESS.

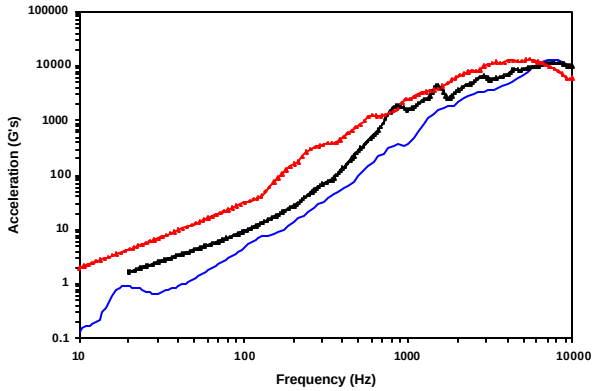

Figure 16 (U) Predicted vs Measured SRS at Front Plate for Sidewall Impact on CGV-FESS.

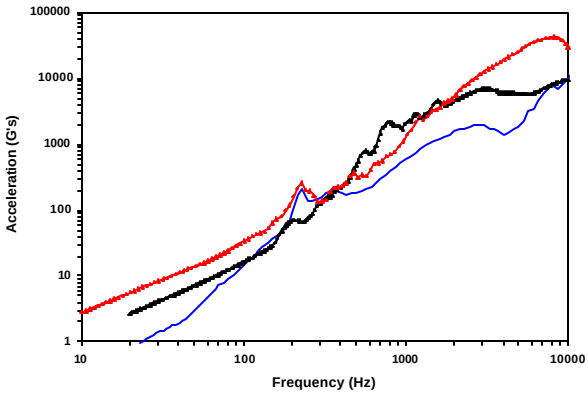

Figure 17 (U) Predicted vs Measured SRS at Sponson Front for Sidewall Impact on CGV-FESS.

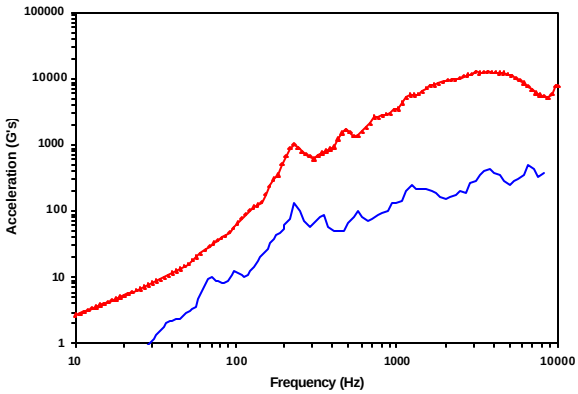

Figure 18 (U) Predicted vs Measured SRS at Inbd Component Base for Sidewall Impact on CGV-FESS.

(U) CONCLUDING REMARKS

(U) The results of this limited analysis demonstrate the relative ease and speed of developing ballistic shock models and predicting shock response in combat vehicles with the SEA approach as compared to FEA model development. The models are easily tuned with measured data such as damping or modal density. Furthermore, the capability to make analytical estimations of contact force and subsystem damping was demonstrated in the end-to-end analysis approach.

(U) The FEA and AutoSEA/PowerSurge predictions were shown to match the test measurements relatively well for the front plate and sponson front response locations. Differences in results are attributed to inaccurate damping estimates, non-linear structural effects, and possibly inaccurate contact load estimation. The inaccuracies in damping estimates are probably due to incorrect assumptions about material behavior and panel size. The force estimates are strongly influence by impact velocity.

(U) Future plans for our research in ballistic shock simulation are, first, to modify the models to agree with test, and understand the mechanisms causing the differences. Second, this analysis method will be used to model the full-up prototype CAV vehicle, which has recently become available. Non-destructive testing will be performed, along with a model tuning exercise. These efforts will demonstrate how the modeling and non-destructive test approach facilitates a disciplined design program, wherein the ballistic shock predictions are refined as the program matures and ultimately well-characterized prior to placement in service.

(U) REFERENCES

1. Dalton, E.C., and B.S. Chambers III, "Analysis and Validation Testing of Impulsive Load Response in Complex, Multi-Compartmented Structures," *Proceedings of the 36th AIAA Structures, Structural Dynamics, and Materials Conference*, 1995.

2. Dalton, E.C., A. Frydman, D. Li, and M. Berman, "High Frequency Shock Predictions in Armored Vehicles: AGS Case Study," *Proceedings of the 16th Int'l Symposium on Ballistics*, San Francisco, CA, September 1996.

3. Dalton, E.C., R.B. Loper, A. Frydman, D. Li, and M. Berman, "Simulation of Ballistic Shock in Composite Armored Vehicles," *Proceedings of the 68th Shock and Vibration Symposium*; 1997.

4. Dalton, E.C., M.D. White, A. Frydman, D. Li, and M. Berman, "Parameter Sensitivity for Statistical Energy Analysis Methods of Ballistic Shock Simulation," *Proceedings of the 69th Shock and Vibration Symposium*, 1998.

5. Dalton, E.C., 1999, *High Frequency Shock Prediction, Short Course Notes*, Sponsored by Military Technology, Inc.

6. Lyon, R.H. and R.G. DeJong, 1995, *Theory and Application of Statistical Energy Analysis, Second Edition*, Butterworth-Heinemann, Newton, MA.

7. Johnson, C.D. and D.A. Kienholz, "Finite Element Prediction of Damping in Structures with Constrained Viscoelastic Layers," *AIAA Journal*, 1982, Vol. 20, No. 9.